ELSEVIER

Catalysis Today 56 (2000) 335–346

CATALYSIS TODAY

www.elsevier.com/locate/cattod

# Surface area and porosity, X-ray diffraction and chemical analyses

E.M. Serwicka (PL-1) *

*Institute of Catalysis and Surface Chemistry, Polish Academy of Sciences ul. Niezapominajek, 30239 Krakow, Poland*

Contributions: J. Kiwi, M. Grätzel (CH-2)[1]; S. Bischof, G.-U. Wolf, M. Baerns (D-1); V. Cortes Corberan, R. Valenzuela (E-1); M. del Arco, C. Martin, V. Rives (E-2); G. Coudurier, W. Desquesnes, P. Mascunan, V. Martin (F-1); J.Ph. Nogier, A.M. De Kersabiec (F-2); H. Praliaud, B. Pommier, J. Varloud (F-3); I. Nova, P. Forzatti (I-3); P. Ciambelli, D. Sannino (I-4); P. K. Olszewski, E.M. Serwicka (PL-1); M. Farinha Portela (PT-1); L.G. Okkel, V.B. Fenelonov, D.A. Zyuzin, E.M. Moroz (RU-1)

**Abstract**

Texture, structure and composition of the fresh and the used EUROCAT oxide $V_2O_5$–$WO_3/TiO_2$ SCR catalysts have been investigated with aid of nitrogen adsorption/desorption at 77 K, mercury porosimetry, X-ray diffraction and chemical analyses. The BET specific surface area is around 47 and 46 $m^2/g$ for the fresh and the used catalyst, respectively. Both samples are essentially mesoporous, with pore diameters centred in the range 10–20 nm according to the data derived from the nitrogen adsorption and around 40 nm according to the mercury porosimetry. The anatase form of $TiO_2$ and traces of orthorhombic $V_2O_5$ are the only crystalline phases identified in both materials. According to the chemical analysis there are no significant differences in the contents of the main constituting elements between the fresh and the used catalyst. Selective dissolution with $NH_3$ aq. reveals that in the used catalyst the amount of vanadium component not susceptible to the treatment increases.


*Keywords:* Surface area; Porosity; X-ray diffraction; Chemical analysis; Selective dissolution

## 1. Introduction

In catalyst characterization, knowledge of the catalyst texture (understood as surface and volumetric characteristics), as well as its phase and chemical compositions, represents an essential minimum. Surface area and porosity evaluation, X-ray diffraction (XRD) and chemical analysis are basic methods providing the required information.

Measurements of gas adsorption isotherms are widely used for determining the surface area and pore size distribution of various solids [1,2]. If the area effectively occupied by an adsorbed molecule is known, the adsorption data may be used to calculate the specific surface from the monolayer capacity of the adsorbent. The use of nitrogen as the adsorptive at 77 K is recommended for determination of surface areas higher than 5 $m^2\,g^{-1}$. The first stage in the interpretation of a physisorption isotherm is to identify the isotherm type and hence the nature of the adsorption processes — monolayer–multilayer formation, capillary condensation or micropore filling. This in turn allows to choose an appropriate procedure for evaluation of the textural properties. It is also necessary that the manner of the isotherm recording follows the IUPAC criteria concerning the experimental set-up and conditions of sample pretreatment [2].

Volumetric characteristics of porous sorbents may be assessed by determination of the pore size distribution and description of the pore shapes. It is usual

* Tel.: +48-12-425-2814; fax: +48-12-425-1923.
*E-mail address:* ncserwic@cyf-kr.edu.pl (E.M. Serwicka (PL-1)).
[1]In association with L. Lucarelli, Thermoquest, Italy.

0920-5861/00/$ – see front matter 
PII: S0920-5861(99)00293-X

to classify pores according to their widths as micropores (less than 2 nm), mesopores (between 2 and 50 nm) and macropores (exceeding 50 nm). The total pore volume is usually derived from the amount of gas adsorbed at a relative pressure close to unity, by assuming that the pores are then filled with condensed adsorptive in the normal liquid state. Several approaches have been developed for the computation of pore size distribution from the adsorption data, all of which involve a number of assumptions, e.g. pore shape, mechanism of pore filling, etc.

Another method used for the determination of the pore size distribution is mercury porosimetry. It is based on the fact that the excess pressure ($\Delta P$) required to force a liquid whose contact angle $\varphi$ with a solid exceeds 90° into a capillary within the solid is related to the capillary size by the expression $\Delta P = (2\gamma/r)\cos\varphi$, where $r$ is the radius of the capillary (assumed cylindrical in form) and $\gamma$ the surface tension of the liquid. Thus, when an outgassed solid is immersed in mercury, a progressive increase of the pressure leads to the penetration of finer and finer pores. The pressures required for assessment of pores in the mesopore and micropore region are very high. To force the mercury into capillaries below 50 nm a pressure of the order of 20 MPa is necessary, and to probe below 20 nm over 350 MPa has to be applied.

XRD analysis is the method most frequently employed for the structural analysis of a solid. It allows to identify in a straightforward manner crystalline phases present in the analyzed material. This can be done by comparing the experimental results with the standard files available from XRD data banks, e.g. ASTM. Analysis of a diffraction pattern allows also to determine the quantities of the XRD detectable phases, unit cell parameters, degree of structural order, size and shape of crystallites and composition of solid solutions.

Chemical analysis provides the information on the elemental composition of the investigated materials. If high accuracy is called for, the "wet" analysis should be performed, which requires dissolution of the solid in an appropriate medium, with subsequent analysis of the solutions with classical or spectroscopic methods. Additional information may be gained by applying a selective dissolution technique which allows to identify the nature (strength) of association of a given component with the bulk of the solid. Chemical analysis may also provide information on the oxidation degree of an element.

Eleven of the 12 laboratories contributing to this section submitted the results of surface area measurements allowing a reasonable evaluation of the scatter of the data. Eight laboratories analyzed the pore size distribution from the nitrogen adsorption isotherms, three measured the pore size distribution by mercury porosimetry, and seven delivered XRD analyses of the samples. Only four laboratories volunteered to provide the full chemical analysis. This is understandable bearing in mind that of the three types of measurements reported in this section the chemical analysis is usually the most time consuming and requires a significant human analytical skill.

## 2. Experimental

### 2.1. Surface area and porosity

The results of surface area and pore size distribution measurements from gas adsorption isotherms were obtained using different types of commercial equipment and home made apparatus which are described in Table 1 together with the sample pretreatment conditions. The samples were used either as pieces of monolith or in a crushed form. Nitrogen was used as the adsorbate.

Mercury porosimetry was performed either with pieces of monolith (I-4) or with crushed material (I-3, CH-2) which, in the case of the experiment performed by CH-2, was additionally disintegrated by the first porosimetry run. The following equipment was used for the measurements: Pascal (0–400 kPa) and Pascal 440 (0.1–400 MPa) of CE Instruments (CH-2), Porosimeter 2000 Series of CE Instruments (0–200 Mpa) (I-3 and I-4).

### 2.2. X-ray diffraction analysis

Samples were used either as monolith pieces or in a powdered form. Following types of diffractometers and experimental conditions were used:

*Laboratory D-1*: STOE STADI P diffractometer, Cu Kα radiation (room temperature), and Nonius Guinnier-Lenné camera, Cu Kα radiation, (25–900°C).

Table 1
BET specific surface areas, BET constant *C*, type of equipment and conditions of sample pretreatment prior to measurement

| Laboratory | Nature of sample | $S_{BET}$ ($m^2\,g^{-1}$) | | $p/p_0$ range | $C_{BET}$ | | Equipment | Pretreatment |
|---|---|---|---|---|---|---|---|---|
| | | Fresh | Used | | Fresh | Used | | |
| CH-2 | Crushed | 45 | 44 | 0.05–0.30 | 125 | 177 | Sorptomatic 1990 Carlo Erba | Vacuum, 150°C, 12 h |
| D-1 | Crushed | 46 | 47 | 0.05–0.25 | 152 | 136 | Gemini III 2375 micromeritics | Vacuum, 400°C, 2 h |
| E-1 | Crushed | 44 | 45 | | 190 | 158 | | Vacuum, 140°C |
| E-2 | Crushed | 46 | 49 | 0.05–0.35 | 133 | 162 | Gemini micromeritics | $N_2$ flow 150°C, 2 h 5 min vacuum |
| F-1 | | 48 | 48 | 0.05–0.23 | 115 | 117 | Home made | Vacuum, 200°C, 2 h |
| F-2 | | 48 | 46 | 0.05–0.20 | 123 | 123 | ASAP 2010 micromeritics | Vacuum, 300°C |
| F-3 | Crushed | 49 | 45 | 0.05–0.35 | 117 | 115 | Home made | Vacuum, 300°C |
| | Monolith | 55 | 48 | | | | | 3 h |
| I-3 | Monolith | 43 | 41 | 0.05–0.33 | | | Sorptomatic 1900 Carlo Erba | Vacuum, 150°C, 12 h |
| I-4 | Monolith | 46 | 46 | 0.05–0.33 | 59 | 104 | Sorptomatic 1990 Carlo Erba | Vacuum, 150°C, 0.5 h |
| PL | Crushed | 45 | 47 | 0.05–0.30 | 98 | 105 | Home made | Vacuum, 200°C, 2 h |
| RU | | 48 | 47 | 0.05–0.20 | 106 | 17 | ASAP 2400 micromeritics | |
| Mean value | | 47 | 46 | | | | | |

*Laboratory E-2*: Siemens D500 diffractometer, graphite-monochromatized Cu Kα radiation.
*Laboratory F-1*: Siemens D5000 diffractometer, graphite-monochromatized Cu Kα radiation.
*Laboratory I-3*: Philips PW 1050/70 diffractometer, Ni-filtered Cu Kα radiation.
*Laboratory I-4*: Philips PW 1710 diffractometer, Ni-filtered Cu Kα radiation.
*Laboratory PL-1*: Siemens D5005 diffractometer, graphite-monochromatized Cu Kα radiation.
*Laboratory PT-1*: Philips diffractometer, Ni-filtered Cu Kα radiation.
*Laboratory RU-1*: Freiberger Präzisionsmechanik GmbH HZG-4 diffractometer, graphite-monochromatized Cu Kα radiation.

In this work XRD analysis was used essentially for a qualitative identification of the crystalline compounds present in the samples. Identification of the crystalline phases was carried out by comparing the experimental results with corresponding ASTM files:

Titanium oxide: 21-1272 (anatase), 21-1276 (rutile), 29-1360 (brookite), 23-1446, 21-1236, 23-606, 33-1381, 34-180, 35-88.
Tungsten oxide: 5-388, 20-1323, 20-1324, 24-747, 32-1393, 32-1394, 32-1395, 33-1387, 37-571.
Vanadium oxide: 9-142, 9-387 (shcherbinaite), 19-1398, 19-1399, 19-1401, 25-1003, 25-1251, 27-1318, 31-1438, 31-1439, 33-1440, 33-1441.
Vanadium tungsten oxide: 22-980, 23-1474, 27-914, 32-1398.

### 2.3. Chemical analysis

The catalysts were dissolved directly or after selective chemical attack by various media. Different procedures, such as melting of the solid with lithium tetraborate, attack with NaOH above its melting temperature or treatment with concentrated acids were used to dissolve the samples. Selective dissolution was performed with aqueous $NH_3$. After total or selective dissolution of the investigated material most elements were analyzed with AES ICP. In some cases colorimetric measurements and potentiometric titration were used.

Details of the experimental procedures applied by various laboratories are given below.

#### 2.3.1. Laboratory D-1

0.010–0.050 g of the sample were mixed with 1 ml 65% $HNO_3$ and 5 ml 40% HF and subjected to a 15 min treatment in a microwave system MDS 2000 (CEM) under a pressure of 8 bar. This resulted in a complete dissolution of the analyzed solids. AES ICP measurement was performed on diluted solutions using the following wavelengths for determination of particular elements: Ti (334, 336 and 337 nm), Si (212, 251 and 288 nm), W (207, 224 and 248 nm), V (270, 292 and 309 nm), Al (394 and 396 nm), Ca (315 and 317 nm).

The mean vanadium valence state was determined by potentiometric titration using a modified method of Niwa and Murakami [3].

*2.3.2. Laboratory F-1*

The samples were grounded before dissolution. For Ti, V, Al and Ca analyses the materials were solubilized by treatment with a mixture of $H_2SO_4$, $HNO_3$ and HF. For the W analysis the samples were dissolved in a mixture of HCl and HF, evaporated and then dissolved in NaOH. Analysis of Si was performed by melting the samples with lithium tetraborate in a Pt–Au crucible at 1100°C, followed by dissolution in 20% HCl. Quantitative determination of the chemical composition was performed with AES ICP analysis.

*2.3.3. Laboratory F-2*

0.1 g of the sample was treated with a mixture of concentrated HCl (20 ml), $HNO_3$ (10 ml) and HF (20 ml) on a sand bath which resulted in a reduction of liquid volume to 5 ml and a complete dissolution of the solids. After dilution with 5% HCl the samples were subjected to the AES ICP analysis using the following wavelengths for determination of particular elements: Ti (338 nm), W (240 nm), V (311 nm), Al (394 and 396 nm).

For determination of Si 0.1 g of the sample was attacked with 1.5 g of NaOH above its melting temperature, dissolved in water and acidified with concentrated HCl. A portion of the solution was used to obtain silico–molybdic complex which, after dilution, was subjected to the measurement of optical density.

Selective attack with aq. $NH_3$ served to determine the amount of soluble V and W and to estimate the fraction of these elements strongly bound to the titania support. It was performed at 60° either in a dynamic or in a static regime using a 1 M ammonia aqueous solution [4,5]. In the first case 0.2 g of the sample was washed dropwise with ammonia solution in a paper filter (of the smallest porosity) at a flow rate of 0.3 ml $min^{-1}$. In one experiment the concentration of dissolved V was continuously followed by potentiometric titration using $Fe^{2+}$ solution, in another both V and W concentrations were analyzed at controlled time intervals with AES ICP method. In a static experiment the sample was subjected to 1 M aq. $NH_3$ treatment for 24 h and the amount of dissolved V and W determined with AES ICP.

*2.3.4. Laboratory F-3*

The elemental analysis was performed by AES ICP method. Different procedures aimed at sample dissolution were used for determination of different elements. Thus, the material solubilized by melting with lithium tetraborate served for analysis of S, Cl, Ti, W, V, Si, Al, Ca and Na. Dissolution in HF followed by treatment with $HNO_3$–$HClO_4$ mixture provided a solution for K and Li analysis. As, Hg, Cd, Pb and Mg were determined after treatment with aqua regia, since the attack with lithium tetraborate is incomplete for these elements. Analysis of several parts of the monolith were performed in order to test the homogeneity. For determination of weight losses upon heat treatment the solids were heated at 1000°C in air, cooled down and kept in a dessicator before weighing.

## 3. Results and discussion

### *3.1. Surface area and porosity*

The specific surface areas gathered in Table 1 were determined by the application of the Brunauer–Emmett–Teller (BET) method. This approach is the most widely used standard procedure for the determination of the surface area of finely divided and porous materials, in spite of the oversimplification of the model on which the theory is based. The BET equation applicable at low $p/p_0$ range is customarily written in the linear form:

$$\frac{p}{n^{a}(p_0 - p)} = \frac{1}{n^{a}_{m}C} + \left(\frac{C-1}{n^{a}_{m}C}\right)\frac{p}{p_0}$$

where $n^a$ is the amount of the gas adsorbed at the relative pressure $p/p_0$, $n^a_m$ the monolayer capacity and $C$ the so-called BET constant which, according to the BET theory, is related to the enthalpy of adsorption in the first adsorbed layer and gives information about the magnitude of adsorbent–adsorbate interaction energy.

Of different possible isotherms the Type II and IV are, in general, amenable to the BET analysis, provided that the value of $C$ is neither too low nor too high, i.e. $20 < C < 200$, and that the BET plot is linear for the $p/p_0$ region taken for calculations.

Both the fresh and the used catalyst gave similar nitrogen adsorption isotherms which differed very little between the laboratories. They corresponded to type IV of the IUPAC classification and showed a characteristic hysteresis loop in the range $p/p_0$ 0.70–0.95

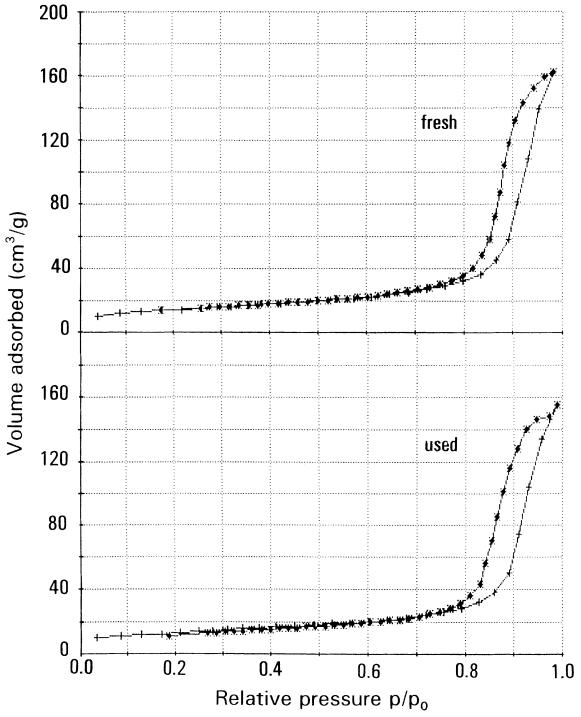


Fig. 1. Nitrogen adsorption/desorption isotherm for (a) fresh and (b) used Eurocat catalyst, recorded by the laboratory F-3.

associated with capillary condensation taking place in mesopores (Fig. 1).

The BET plots show excellent linearity, with a correlation factor of 0.9999 (Fig. 2). The results calculated on the basis of isotherms obtained by different laboratories are summarized in Table 1.

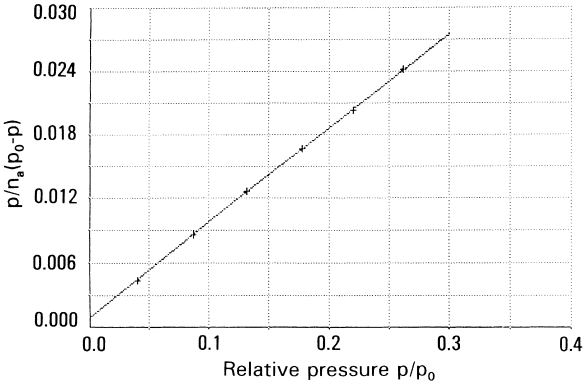


Fig. 2. BET plot obtained for a fresh Eurocat catalyst by the laboratory F-3.

The data show clearly that, independent on the used equipment, there is, essentially, a good agreement in the specific surface areas determined by different laboratories, the average value being 47 and 46 $m^2\,g^{-1}$ for the fresh and the used catalyst, respectively. Also, the nature of the sample, i.e. monolith or crushed, had no significant influence on the obtained results. Laboratory F-3, who analyzed both types of material, observed that a measurement performed on a crushed material gave specific surface areas by ca. 10% lower. The values of BET constant *C* gathered in Table 1 range from 59 to 190 for fresh and from 17 to 177 for used samples. This may be taken as an indication that basically monolayer–multilayer formation is operative and is not accompanied by any meaningful micropore filling which is usually associated with an increase in the value of *C* above 200.

A number of approaches (*t*, $\alpha_s$, BJH, DFT, Dollimore–Heal, Cranstone–Inkley and Roberts methods) were used to assess the micro- and the mesoporosity from the adsorption data. Most of the contributors, except of F-2, found no micropores in the investigated materials and described the samples as essentially mesoporous. Laboratory F-2 deduced from the *t*-plot analysis a small contribution from micropores of 0.7 nm mean diameter and surface area of 3.7 $m^2\,g^{-1}$. Pore size distribution curves recorded by laboratories CH-2, D-1, E-2, F-3, I-3, I-4 and RU-1 demonstrated that the major contribution stems from pores with diameter in the range 10–20 nm, as illustrated in Fig. 3. All measurements showed that the catalyst maintained its mesoporous characteristics after use in the catalytic conditions, the pore size distribution curves having very similar shape for the fresh and the used catalyst. Several laboratories (F-2, I-4 and RU-1) performed the pore distribution calculations for both the desorption and the adsorption branches and found significant differences in the results. This has been clearly demonstrated by the laboratory I-4 which compared the assessment of mesoporosity, from both the adsorption and the desorption data, using different methods based on different models. The results gathered in Table 2 show that when the desorption data are used for calculations lower values of pore sizes are obtained, irrespective of the method applied for the pore size evaluation. This shows the inadequacy of cylindrical or slit-shape model in evaluating the pore size distribution. Laboratory F-3 found that

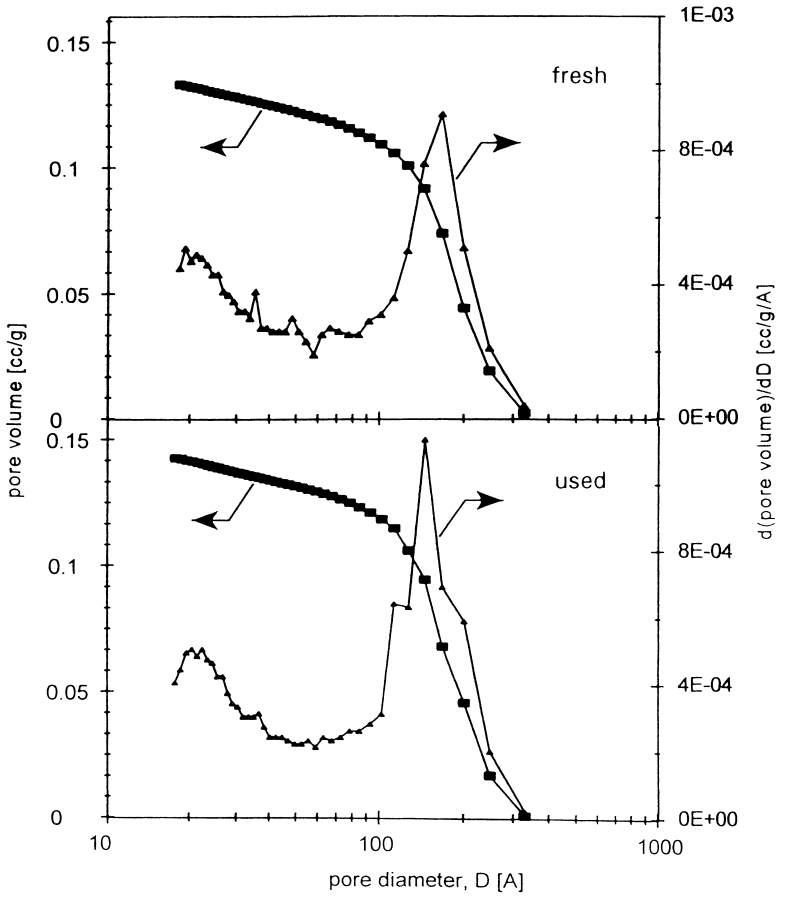


Fig. 3. Pore size distribution and cumulative pore volume obtained from the nitrogen desorption isotherms for the fresh and the used catalyst by the laboratory D-1 (BJH method).

the cumulative surface areas and the cumulative pore volumes deduced from the Robert's method based on a cylindrical pore model are higher than the BET surface areas and adsorbed volumes at saturation and suggested that some bottle shape pores may occur.

The pore size distribution of the catalysts was also assessed with the aid of mercury porosimetry, assuming a cylindrical pore model and using the Washburn equation (CH-2, I-3, I-4). Table 3 summarizes the average pore sizes and cumulative pore volumes obtained by different contributors. All laboratories found a monomodal pore distribution in the mesopore range with a maximum centered around a pore radius of 20 nm (pore diameter 40 nm) (Fig. 4). Also the cumulative volume of pores in the range below 50 nm is in all cases similar, so the data on the mesoporosity are consistent. Differences arise in the area of macroporosity. Laboratory CH-2 found a maximum centered around 6 μm, while no such maximum was observed by the remaining two contributors. This is most probably due to the different manner of sample pretreatment resulting in different fragmentation of the monolith. In particular, laboratory I-4 used a piece of monolith in their measurement, while laboratory CH-2 worked with a crushed material, additionally disintegrated by the first experimental run. The lower upper limit of pore size measurement set by laboratory I-3 ($8 \times 10^3$ vs $5 \times 10^4$ nm chosen by I-4 and CH-2) resulted in the lower total cumulative volume found in their experiment. Nevertheless, irrespective of the differences between the laboratories in the assessment of the macropore range, the similarity of the

Table 2
Evaluation of pore size distribution from the adsorption or desorption branches in the range 0.6–0.95 $p/p_0$ for the Eurocat catalyst using different methods (*t*-correction Harkins–Jura) performed by the laboratory I-4

| Method | Porosity parameters | Fresh | Used |
|---|---|---|---|
| BJH adsorption | Pore volume ($cm^3\,g^{-1}$) | 0.118 | 0.111 |
| | Mean pore size (nm) | 18.7 | 17.6 |
| | Pore size maximum (nm) | 21.6 | 22.0 |
| BJH desorption | Pore volume ($cm^3\,g^{-1}$) | 0.269 | 0.1674 |
| | Mean pore size (nm) | 15.9 | 15.8 |
| | Pore size maximum (nm) | 13.5 | 14.8 |
| Cranston and Inkley adsorption | Pore volume ($cm^3\,g^{-1}$) | 0.121 | 0.119 |
| | Mean pore size (nm) | 18.4 | 22.7 |
| | Pore size maximum (nm) | 21.6 | 21.3 |
| Cranston and Inkley desorption | Pore volume ($cm^3\,g^{-1}$) | 0.269 | 0.254 |
| | Mean pore size (nm) | 15.9 | 15.8 |
| | Pore size maximum (nm) | 13.6 | 14.8 |
| Dollimore and Heal adsorption | Pore volume ($cm^3\,g^{-1}$) | 0.118 | 0.120 |
| | Mean pore size (nm) | 18.6 | 22.6 |
| | Pore size maximum (nm) | 21.8 | 21.2 |
| Dollimore and Heal desorption | Pore volume ($cm^3\,g^{-1}$) | 0.268 | 0.167 |
| | Mean pore size (nm) | 16.0 | 15.9 |
| | Pore size maximum (nm) | 13.6 | 14.8 |
| Modelless (BMD) adsorption | Pore volume ($cm^3\,g^{-1}$) | 0.122 | 0.129 |
| | Mean pore size (nm) | 4.2 | 4.1 |
| | Pore size maximum (nm) | 4.8 | 5.1 |
| Modelless (BMD) desorption | Pore volume ($cm^3\,g^{-1}$) | 0.280 | 0.176 |
| | Mean pore size (nm) | 3.0 | 3.2 |
| | Pore size maximum (nm) | 2.6 | 3.3 |

recorded profiles for the new and the used catalysts observed by a given laboratory indicates that both the intra- and the inter-particle pore structures of the catalyst are stable in the reaction conditions.

### 3.2. X-ray diffraction analysis

XRD patterns obtained in different laboratories were similar. No significant differences between the fresh and the used catalyst were observed, indicating that the reaction environment did not affect the crystalline structure of the catalyst (Fig. 5a). Only the presence of $TiO_2$ (anatase) has been detected in both studied materials by most laboratories. This phase was observed without peak shifts. No contribution from rutile could be observed at room temperature. In some cases (E-2, PL-1, PT-1, RU-1) some X-ray lines of weak intensity were observed in the $2\theta$ region between 15° and 32° associated, according to E-2, PL-1 and PT-1, with the presence of $V_2O_5$. Laboratory

Table 3
Average intra-particle pore radius and cumulative pore volumes as obtained from mercury porosimetry

| Laboratory | Radius (nm) | | Volume ($R < 50$ nm) ($cm^3\,g^{-1}$) | | Volume (total) ($cm^3\,g^{-1}$) | |
|---|---|---|---|---|---|---|
| | Fresh | Used | Fresh | Used | Fresh | Used |
| CH-2 | 22 | 22 | 0.27 | 0.27 | 0.50 | 0.58 |
| I-3 | 20 | 20 | 0.24 | 0.21 | 0.27 | 0.24 |
| I-4 | 22 | 22 | 0.25 | 0.27 | 0.40 | 0.42 |

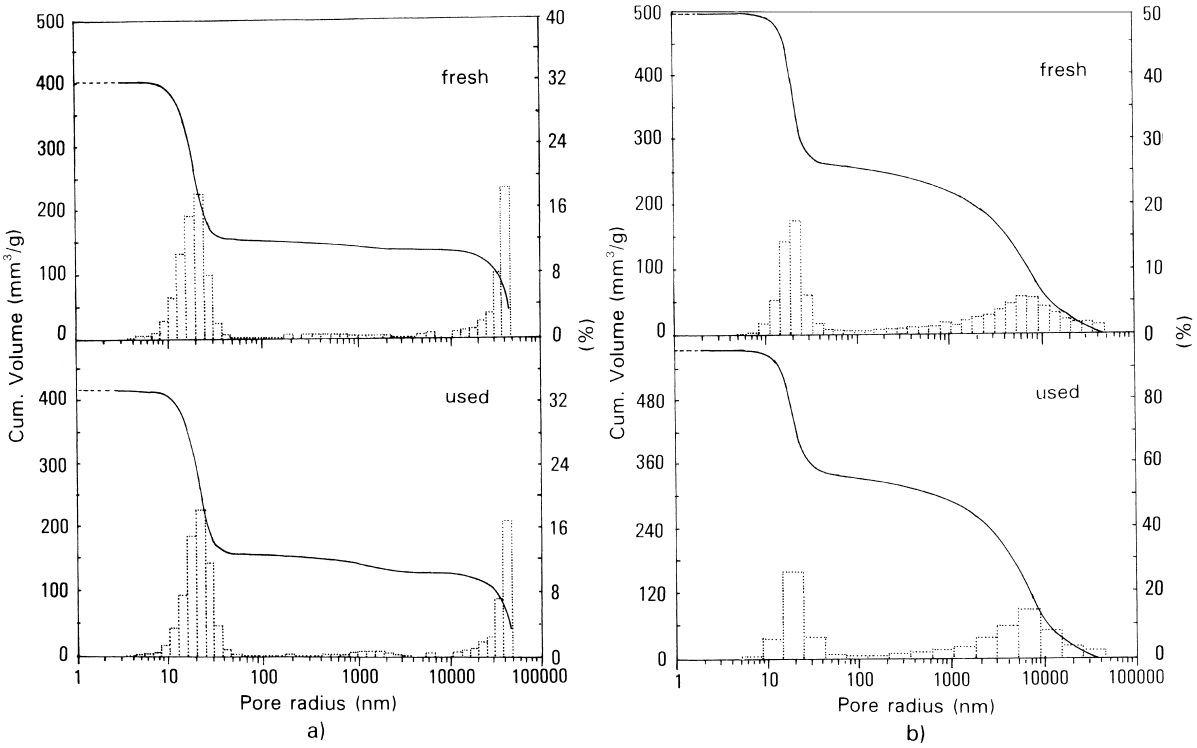


Fig. 4. Pore size distribution and cumulative pore volume obtained from mercury porosimetry for the fresh and the used catalyst (a) by the laboratory I-4, monolith (b) by the laboratory CH-2, crushed.

PL-1 was able to identify most of these reflections as belonging to the orthorhombic form of this oxide (ASTM 9-387) (Fig. 5b). A peak at $2\theta = 19.9^\circ$, pointing to the existence of yet another phase, remained unidentified. In the samples subjected to heating to 900°C only the anatase to rutile transformation was observed with no sign of crystallization of any possible amorphous phases (D-1).

The Scherrer equation with Warren correction was used for estimation of the mean crystallite size of $TiO_2$ (F-1, I-3). Table 4 shows the results obtained by laboratory F-1 for different crystal planes. The sizes of $TiO_2$ crystallites are between 20 and 30 nm. The relatively weak dependence of the crystallite size on the crystal plane indexes indicates that the particles are of spherical or slightly ovoid shape. Bearing in mind the theoretical approximations and experimental limitations the calculated values are given with the accuracy of ±20–30%. Consequently, there are no significant differences in the values obtained for the new and the used catalyst. Laboratory I-3 pointed out that the mean size of titania particles is compatible with the mean mesopore diameter found by nitrogen adsorption, indicating that the observed mesoporosity is the result of voids between the single support crystallites.

### 3.3. Chemical analysis

#### 3.3.1. Elemental composition

The results of the elemental analysis for the dominant components present in the fresh and the used samples are gathered in Tables 5 and 6, respectively. In most cases a fairly good agreement is observed for the data obtained for a given element by different laboratories, and the analyses show good reproducibility. The mean standard deviation $\sigma$ constitutes in most cases less than 10% of the average value. Noticeable scatter with $\sigma$ equal to ca. 20% or more of the mean value occurs in the determination of W, Al and Ca. High $\sigma$ for determination of W is due to the fact that one of the analyses reported by laboratory F-3 gave significantly higher W content. In the case of Al and

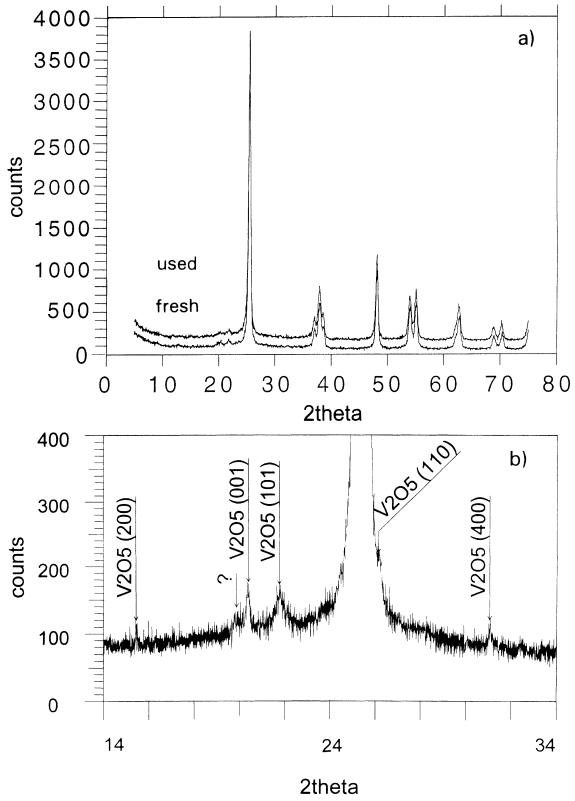


Fig. 5. (a) XRD patterns of fresh and used Eurocat catalyst obtained by the laboratory E-2; (b) assignment of weak reflections in the $2\theta$ range 15–32° to the orthorhombic form of $V_2O_5$, performed by the laboratory PL-1.

Ca determination the values given by laboratory F-2 were higher than the analyses produced by D-1, F-1 and F-3. The most probable reason for the scatter of the data is the inhomogeneous distribution of the concerned elements in the investigated solid, but some analytical problems have to be taken into account as well.

Table 4
Size of $TiO_2$ crystallites calculated from the XRD pattern by the laboratory F-1

| $2\theta$ (deg) | Plane indexes (*hkl*) | Crystallite size (nm) | |
|---|---|---|---|
| | | Fresh | Used |
| 25.3 | 101 | 22 | 20 |
| 48.0 | 200 | 30 | 25 |
| 53.9 | 105 | 27 | 17 |
| 55.0 | 211 | 28 | 25 |
| 62.6 | 204 | 20 | 25 |

For instance, laboratory F-2 noticed that the results of Al determination varied strongly with the wavelength used for ICP analysis and suggested that the presence of some undetermined elements perturbed their analysis. This laboratory also pointed out that in the case of W determination severe problems associated with the sample dissolution have to be taken into account as possible reasons for erroneous analysis. $WO_3$ is essentially insoluble in acidic media and for this reason the acidified W solutions of concentration higher than ca. $10^{-4}$ mol $l^{-1}$ are unstable and yield eventually a $WO_3$ precipitate. This has to be borne in mind when preparing both the solutions of the analyzed material and the standard solutions for AES ICP measurement. This problem can be avoided when the sample is dissolved by melting with lithium tetraborate, as performed by the laboratory F-3.

The mean vanadium valence state determined by laboratory D-1 was 4.77 and 4.79 in the fresh and the used Eurocat catalysts, respectively.

From Tables 5 and 6 it follows that the W/Ti and V/Ti atomic ratios were equal, 0.038 and 0.041, respectively, for the fresh catalyst, and 0.042 and 0.045 for the used sample.

Laboratory F-1 also analyzed the so-called “titania support” used for the deposition of the active phase (Table 7). The results have shown that the carrier contains, beside titanium, also W, Si, Al and Ca in similar quantities as in the final catalyst, except for vanadium which appears only in a trace amount.

Besides the main components listed above, the Eurocat catalyst was found to contain several other elements in lesser amounts. These were: Fe (0.20–0.25 wt.%), S, whose quantity in the fresh catalyst was smaller (0.12–0.24 wt.%) than in the used one (0.23–0.36 wt.%), Mg (0.14–0.17 wt.%), Hg (0.13–0.23 wt.%), Na (0.2 wt.%), Pb (0.01–0.13 wt.%), Cl (<0.1 wt.%), K (0.02 wt.%), Li (0.02 wt.% or less), As (<0.01 wt.%) and Cd (<0.01 wt.%) (according to Laboratory F-3). Laboratory D-1 found Fe (0.14–0.17 wt.%), Nb (0.07 wt.%), Zr (0.03 wt.%) and Mn (<0.01 wt.%).

Generally, no significant differences in the contents of the main components between the fresh and the used catalyst have been found.

Laboratory F-3 found the weight loss at 1000°C to be 2.65 and 2.80% for fresh and used catalyst, respectively.

Table 5
Elemental composition of fresh Eurocat catalyst (main components X = Ti, W, Si, V, Al, Ca)

| Laboratory | Ti (wt.%) | W (wt.%) | Si (wt.%) | V (wt.%) | Al (wt.%) | Ca (wt.%) |
|---|---|---|---|---|---|---|
| D-1 | 44.9 | 6.3 | 4.8 | 2.0 | 1.0 | 1.4 |
| | 45.6 | 6.6 | 4.4 | 2.0 | 1.0 | 1.4 |
| F-1 | 42.8 | 6.6 | 4.6 | 1.7 | 1.0 | 1.2 |
| | 42.1 | 6.5 | 4.6 | 1.7 | 1.0 | 1.2 |
| F-2 | 42.6 | 5.7 | 4.7 | 2.1 | 2.6 | 1.9 |
| | 44.3 | 5.9 | 4.5 | 2.1 | 2.4 | 1.8 |
| | 43.2 | 5.8 | | 2.1 | 3.0 | 2.1 |
| F-3 | 39.7 | 9.4 | 4.5 | 2.0 | 1.0 | 1.5 |
| | 43.3 | 5.6 | 5.1 | 1.9 | 1.1 | 1.5 |
| | 43.0 | 5.8 | | 1.7 | | |
| | 43.2 | 5.4 | | 2.0 | | |
| Mean value | 43.2 ($\sigma = 1.5$) | 6.3 ($\sigma = 1.1$) | 4.7 ($\sigma = 0.2$) | 1.9 ($\sigma = 0.2$) | 1.6 ($\sigma = 0.8$) | 1.6 ($\sigma = 0.3$) |
| X/Ti atomic ratio | 1.000 | 0.038 | 0.185 | 0.041 | 0.067 | 0.044 |

Table 6
Elemental composition of used Eurocat catalyst (main components X = Ti, W, Si, V, Al, Ca)

| Laboratory | Ti (wt.%) | W (wt.%) | Si (wt.%) | V (wt.%) | Al (wt.%) | Ca (wt.%) |
|---|---|---|---|---|---|---|
| D-1 | 45.4 | 6.5 | 4.8 | 2.1 | 1.0 | 1.3 |
| | 45.5 | 6.6 | 4.4 | 2.1 | 1.0 | 1.4 |
| F-1 | 42.7 | 6.6 | 4.6 | 1.7 | 1.0 | |
| | 42.4 | 6.4 | 4.7 | 1.8 | 1.0 | 1.2 |
| F-3 | 42.0 | 10.4 | 4.0 | 2.4 | 1.2 | 1.9 |
| | 43.0 | 4.7 | | 2.4 | | |
| Mean value | 43.5 ($\sigma = 1.4$) | 6.9 ($\sigma = 1.7$) | 4.5 ($\sigma = 0.3$) | 2.1 ($\sigma = 0.3$) | 1.0 ($\sigma = 0.1$) | 1.5 ($\sigma = 0.3$) |
| X/Ti atomic ratio | 1.000 | 0.042 | 0.176 | 0.045 | 0.041 | 0.041 |

### 3.3.2. *Selective attack with aq. $NH_3$*

Chemical attack of the samples was performed by the laboratory F-2 at 60°C with a 1 M ammonia aqueous solution either by flowing the solution at a rate of $0.3\,cm^3\,min^{-1}$ for a kinetic study or in static conditions for a stronger attack. Fig. 6a shows the kinetics of V and W dissolution for the fresh sample in dynamic conditions and Fig. 6b the comparative kinetics of V dissolution for the fresh and used samples. It appears that after a fast attack the process tends slowly to asymptotic values.

For the fresh sample one obtained dissolution, expressed in $10^{-5}\,mol\,g^{-1}$, of ca. 12.5 (34% V) and 2.3 (6.5% W) after 15 min, of ca. 15 (40% V) and 3.1 (9%

Table 7
Elemental composition of "support" used for manufacturing of the Eurocat catalyst (main components X = Ti, W, Si, V, Al, Ca)

| Laboratory | Ti (wt.%) | W (wt.%) | Si (wt.%) | V (wt.%) | Al (wt.%) | Ca (wt.%) |
|---|---|---|---|---|---|---|
| F-1 | 43.3 | 6.7 | 4.3 | 0.1 | 1.0 | 1.2 |
| | 44.2 | 6.4 | 4.1 | 0.1 | 1.0 | 1.2 |
| Mean value | 43.8 ($\sigma = 0.5$) | 6.6 ($\sigma = 0.2$) | 4.2 ($\sigma = 0.1$) | 0.1 ($\sigma = 0$) | 1.0 ($\sigma = 0$) | 1.2 ($\sigma = 0$) |
| X/Ti atomic ratio | 1.000 | 0.039 | 0.163 | 0.002 | 0.040 | 0.033 |

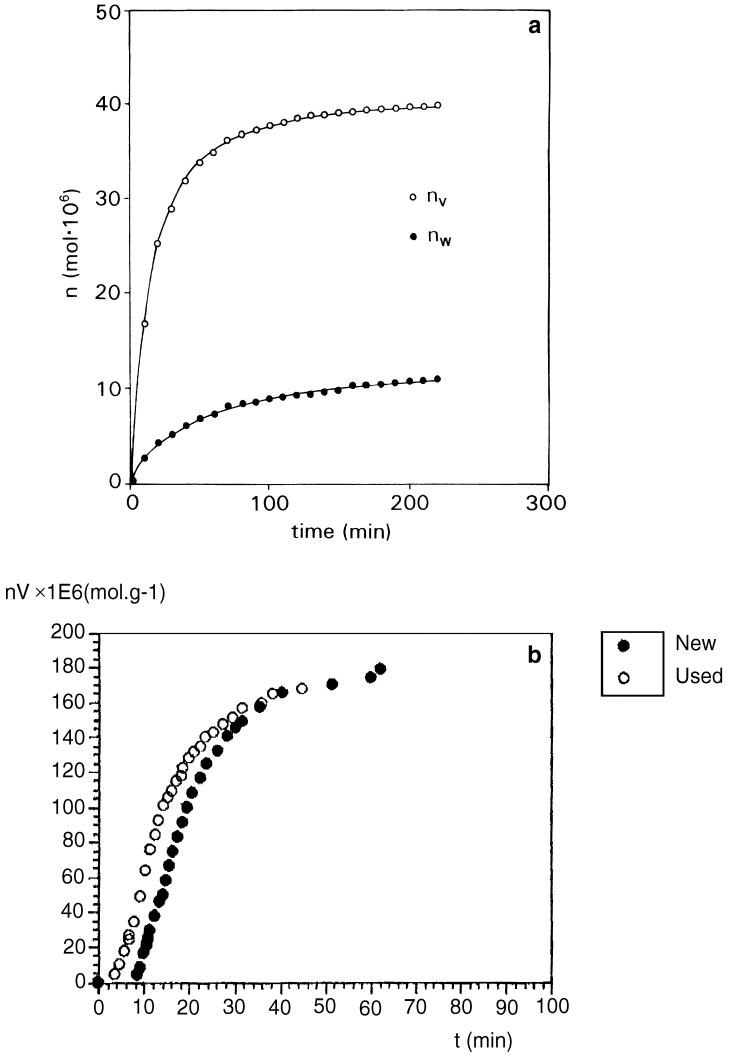


Fig. 6. (a) Kinetics of V and W dissolution upon treatment with aq. $NH_3$ in a dynamic regime for the fresh Eurocat catalyst (sample weight 0.1778 g); (b) comparison of V dissolution kinetics for the fresh and the used sample, obtained by the laboratory F-2.

W) after 30 min, of ca. 17.4 (47% V) and 4.5 (13% W) after 1 h and of ca. 22 (59% V) and 6.2 (18% W) after 3 h in dynamic conditions. In the static conditions the dissolution of ca. 27 (72% V) after 12 h and of ca. 33 (88% V) and 8.5 (25% W) after 24 h was obtained.

For the used sample one obtained dissolution of ca. 12.5 (30% V) after 15 min and of ca. 17.2 (42% V) after 1 h in dynamic conditions, and of 25% (61% V) after 12 h in static conditions.

Several important conclusions can be drawn:

1. Large amounts of vanadium and, to a smaller extent, tungsten ions are dissolved rapidly, the used sample giving smaller values in the whole study, even if the accuracy of the technique could be questioned. The former point may indicate that V ions and, to a much lesser extent, W ions are localized in a few top layers of the catalyst particles. The latter point is coherent with the data from XPS and electrical conductivity mea-

surements, presented in the following chapters, which showed that V ions become more incorporated in the bulk of the particles after industrial operation.

2. The majority of the W cations but the minority of the V cations are strongly bound to $TiO_2$ particles, since after 24 h chemical attack it was observed that 75 mol% of tungsten and 12 mol% of vanadium are resistant to the selective attack with aq. $NH_3$. The results of the XPS and the electrical experiments indicate that the species unaffected by treatment with ammonia are deeply embedded in titania matrix.

## 4. Conclusions

### *4.1. Surface area and porosity*

The BET specific surface area is around 47 and 46 $m^2\,g^{-1}$ for the new and the used catalyst, respectively. Both samples are essentially mesoporous, with pore diameters centered in the range 10–20 nm according to the data derived from the nitrogen adsorption isotherm and around 40 nm according to the mercury porosimetry. The intra- and inter-particle structure remains basically unaffected by working under catalytic conditions.

### *4.2. X-ray diffraction analysis*

The anatase form of $TiO_2$ and traces of orthorhombic $V_2O_5$ are the only crystalline phases definitely identified in both investigated samples. No shifts are observed in the positions of the anatase reflections. Titania crystallites are spherical or slightly ovoid in shape, of dimensions between 20 and 30 nm. This suggests that the mesoporosity observed in the samples stems from voids between the support crystallites.

### *4.3. Chemical analysis*

A fairly good agreement is observed for the quantitative determination of the majority of dominant elements performed by different laboratories. Some scatter of the data observed in the case of W, Al and Ca determination is probably associated with the inhomogeneous distribution of these elements in the bulk of the catalyst, but in some cases analytical problems have been reported. As most of the analytical data are obtained with the AES ICP technique it is vital to provide the details on the sample dissolution, method of standard preparation, and λ used for determination of a particular element. In the case of W determination it has to be borne in mind that the solubility of tungsta in acidic media is very limited. For this reason a particular care has to be taken when preparing both the solutions for analysis and the standard ICP solutions.

The experiments with the selective dissolution show that a prolonged exposure to ammonia solution affects vanadium and tungsten in a different manner. While most of the vanadium undergoes dissolution, the majority of tungsten remains unaffected. In view of the XPS and electrical conductivity measurements presented in the following chapters, the parts of vanadium (minority) and tungsten (majority) resistant to dissolution are deeply embedded in titania particles. In the used catalyst the amount of vanadium not susceptible to dissolution increases.

## References

[1] S. Gregg, K.S.W. Sing, Adsorption, Surface Area and Porosity, Academic Press, New York, 1982.
[2] K.S.W. Sing, D.H. Everett, R.A.W. Haul, L. Moscou, R.A. Pierotti, J. Rouquerol, T. Siemieniewska, Pure Appl. Chem. 57 (1985) 603.
[3] M. Niwa, Y. Murakami, J. Catal. 76 (1982) 9.
[4] J.Ph. Nogier, J. Thoret, N. Jammul, J. Fraissard, Appl. Surf. Sci. 47 (1990) 287.
[5] J.Ph. Nogier, Compiler, Catal. Today 20 (1994) 23.